Journal Pre-proofs

Mixing in flows past confined microfluidic cylinders: effects of pin and fluid interface offsetting

Shigang Zhang, Neil Cagney, Tom Lacassagne, Stavroula Balabani, Carolina P. Naveira-Cotta, Manish K. Tiwari

Please cite this article as: S. Zhang, N. Cagney, T. Lacassagne, S. Balabani, C.P. Naveira-Cotta, M.K. Tiwari, Mixing in flows past confined microfluidic cylinders: effects of pin and fluid interface offsetting, *Chemical Engineering Journal* (2020), doi: https://doi.org/10.1016/j.cej.2020.125358

Mixing in flows past confined microfluidic cylinders: effects of pin and fluid interface offsetting

Shigang Zhang[a,b], Neil Cagney[b,e], Tom Lacassagne[b], Stavroula Balabani[b], Carolina P. Naveira-Cotta[a,c], Manish K. Tiwari[a,d,*]

[a] *Nanoengineered Systems Laboratory, Department of Mechanical Engineering, University College London (UCL), London, WC1E 7JE, UK*

[b] *Department of Mechanical Engineering, University College London (UCL), London, WC1E 7JE, UK*

[c] *Mechanical Engineering Department (PEM) & Nanoengineering Department (PENT), Federal University of Rio de Janeiro-UFRJ, Rio de Janeiro, RJ, Brazil*

[d] *Wellcome/EPSRC Centre for Interventional and Surgical Sciences, University College London (UCL), London, UK*

[e] *School of Engineering and Materials Science, Queen Mary University of London*

ABSTRACT

Inserting obstacles such as cylindrical pins in a micromixer has the potential to significantly enhance scalar transport and improve species mixing between two co-flowing streams. However, it remains unclear how the mixing efficiency in confined microchannel flows is affected by the positioning of the fluid interface and the cylindrical pin with respect to the wall or to each other. The present work investigates the mixing induced by a single cylindrical pin placed at different gap distances from the wall of a Y-

---

[*] Corresponding author. Email: m.tiwari@ucl.ac.uk. Phone: +44 20 3108 1056.

type micromixer. Two fluid interface positions are considered by mixing the fluid streams at different ratios; one located at the channel centreline and one shifted towards one of the walls. Micro particle image velocimetry (µPIV) is applied to investigate the velocity fields and streamline patterns for the different pin locations, and micro laser-induced fluorescence (µLIF) to acquire the instantaneous concentration fields and assess the mixing performance, utilising the intensity of segregation technique. Prior to the onset of vortex-shedding and when the fluid interface coincides with the channel centreline, slightly offsetting the pin from the centreline is found to yield the best mixing performance compared to centreline or near wall pin locations. However, when vortex-shedding is present, a centreline pin location exhibits the best mixing performance. The present measurements indicate that single micropins can enhance mixing, even in the absence of vortex-shedding, and when vortex-shedding occurs, they are most efficient when the pin axis and fluid interface are aligned.

1. Introduction

Mixing at small length scales such as those encountered in microfluidic devices is inherently challenging because diffusion tends to dominate in such laminar flows [1,2]. Inserting obstacles such as cylindrical pins into a microfluidic channel is a promising means of promoting chaotic advection, and hence mixing, heat and mass transfer, and has thus been of great interest in various applications, including chemical reactors [3,4] and electronics cooling [5].

The flow past a cylinder is one of the most widely studied problems in fluid mechanics, due to its relevance throughout both industry and nature. However, unlike its macroscale counterpart, described in detail in many seminal works [6–8], the flow past a cylinder in a microfluidic channel typically experiences some unique features such as high blockage (ratio of cylinder diameter to channel width) and a low aspect ratio (cylinder length to diameter ratio) [9] due to the size limitation of microfluidic devices, which is in the sub-millimeter range [10]. Thus, cylindrical obstacles in micromixers are bounded both by the side and top walls, i.e. they are both laterally and vertically confined, and the flow is inherently modified by this confinement, as the latter can suppress vortex-shedding [11]. The lateral and vertical confinement in such micro-confined cylinder flows can be expressed in terms of $w^* = W/D$ and $h^* = H/D$ respectively, where W is the channel width, H the height and D the cylinder diameter. These correspond to the reciprocal of the blockage ratio and the aspect ratio respectively, that are commonly used in macroscale flows past cylinders. Nevertheless, vortex-shedding can be induced in such confined microchannels at sufficiently high Reynolds number ($Re = U_o D_h / u$, where U_o is the mean freestream velocity in the channel, D_h is the hydraulic diameter of microchannel and u is the kinematic viscosity of the fluid) as

3

shown in our previous work [11], inducing periodic changes in the local direction of the flow. Flow vortices are excellent candidates to further increase mixing through stretching and folding of the species streams [12]. Thus, the mixing induced by microfluidic cylinders is expected to depend both on geometrical as well as flow parameters (e.g. *Re*) and a systematic investigation of these parameters is still lacking.

The degree of mixing in a flow can be quantified through various techniques and indices, such as the intensity of segregation [13,14], Lyapunov exponents [15], the iodide–iodate reaction [16], striation thickness [17] and Shannon entropy [18]. The intensity of segregation, *I*, is a widely used approach to assess the global mixing performance of micromixers and provides a measure of the inhomogeneity of a mixture. When considering the mixing of two liquid components with the same physical properties (density, viscosity etc.), we can write:

$$I = \frac{\sigma_c^2}{\overline{C}\,(1 - \overline{C})} \tag{1}$$

where σ_c and $\overline{C}$ respectively are the standard deviation and mean of the normalized concentration of a single component over a given region. This is often expressed in terms of the mixing index, *M*, with expression as [19]:

$$M = 1 - \sqrt{I} \tag{2}$$

with *M* = 1 indicating a perfectly mixed (homogeneous) fluid, and *M* = 0 indicating a completely segregated mixture. The literature on mixing in passive micromixers with obstacles focusses on arrays rather than single obstacles. For example, Bhagat et al. [20] investigated the effect of obstacle height, shape and offset on mixing in microchannels with obstacle arrays at Reynolds number (*Re*) ranging from 0.01 to 100 (numerically) and 0.02 to 10 (experimentally). The best mixing was found for microchannel geometries with obstacles spanning the full microchannel height,

arranged in an alternate fashion across the channel off the centreline and with a diamond shape. Chen et al. [10] experimentally investigated the mixing in a channel with a high-density array of 15 μm pillars ($w^* = 13$ and $h^* = 3$) at Reynolds number ranging from 0.1 to 6.8. They observed a reduction of mixing in the range Re = 0.1 - 0.68 but the mixing index remained constant when Re increased to 6.8. Tseng et al. [21] carried out numerical simulations on diamond-shaped obstacles in microchannels with a similar geometry to that used in the study of Bhagat et al.[20], and observed that better mixing is attained at low Re (~0.1) due to enhanced diffusion and at higher Re (~50) due to enhanced convection; however, mixing was relatively poor in intermediate Re ranges ($0.5 < Re < 10$). Cetkin and Miguel [22] numerically investigated the effect of inlet angles in the micromixers with and without circular obstacles inserted in staggered arrangement at Re of 100. Compared to the micromixer without obstacles, strong flow impedance and good mixing performance (over 70%) was observed in the micromixers with obstacles and the inlet angles had a negligible effect on the mixing efficiency as well as the flow impedance. Dundi et al. [23] carried out numerical simulations of the flow in a micromixer with circular obstructions ($D = 25$ μm, $w^* = 8$ and $h^* = 4$) at Re ranging from 6 to 700. They observed that the mixing index increased monotonically with Reynolds number increasing from 100 to 700. However, they did not report any data or discuss whether vortex-shedding was present at this relatively high Re.

Most studies on passive micromixers with obstacles assume that the fluids are mixed at a ratio of 1:1, i.e. the interface between the fluid streams coincides with the microchannel centreline. However, in many practical applications, the interface between the two mixing fluids does not necessarily lie at the microchannel centreline.

A typical example is when dealing with different molar ratio and/or flow rate of reactants, as in biodiesel synthesis in microreactors [24,25]. In accordance with the standard ASTM D6751-15 [26], biodiesel is made up by mono-alkyl esters of long-chain fatty acids fuel, derived from vegetable oils and/or animal fats, commonly produced via transesterification reaction. The molar ratio of alcohol to oil is one of the most important parameters affecting the yield of alkyl ester [27,28], which clearly indicates the importance of studying the mixing induced when varying the location of the fluid interface (associated with variations in the reactant molar ratios and flow rates).

Offsetting the fluid interface in simple Y-type micromixers, i.e. in the absence of obstacles, has shown conflicting results in the literature. For example, Ansari et al. [29] numerically investigated the dependency of the mixing index on the fluid interface position, expressed as the fraction of a (rectangular) channel width occupied by one of the streams (l/W, see Fig. 1 for definition). They observed that the mixing index decreased from 50% to 10% with l/W decreasing from 0.5 (interface at channel centreline) to 0.2 at low Re (< 0.1) but showed a slight change for Re number over 5. Viktorov et al. [30] numerically investigated the mixing performance in a split-and-recombine micromixer with inlet flow rate ratios of 1:1 to 3:1 at Re ranging from 10 to 100. They observed that the ratio of 3:1 exhibited better mixing than the 1:1 ratio for 10 < Re < 40. However, the inlet flow rate ratio had a negligible effect at relatively high Reynolds number range (60 < Re < 100) as the mixing index reached over 90% in this regime. There is a paucity of experimental data in the literature on the dynamics of mixing in microscale flows with varying positions of the fluid interface. In particular, there remain some unresolved questions regarding the position of fluids interface (or

6

flow ratio of the two streams) in micromixers with obstacles, such as: does the change of fluids interface position significantly affect the mixing performance? Can offset the obstacle from the channel centreline and towards the fluids interface help mixing in applications where the flow ratio differs from 1:1?

Offsetting an obstacle from the centreline and towards the channel walls is expected to alter the flow past it. In the case of cylindrical obstacles, evidence from the literature on flows past a circular cylinder near a single plane boundary suggests that asymmetric flows can be generated and vortex-shedding suppressed, due to the wall proximity. Lei et al. [31] found numerically that the vortex-shedding was delayed when the gap ratio, $\delta = g/D$, (where g is the gap distance between the pin and the channel wall, as shown in Fig. 1) between the cylinder and the wall became smaller than 0.3 ($\delta < 0.3$). Zovatto and Pedrizzetti [32] also found (through 2D numerical simulations) that the close proximity of the wall can inhibit the appearance of vortex-shedding and reduce the length of the separating shear layer as δ decreased from 2 to 0.25. Similar findings have been reported in the experimental studies by Wang and Tan [33] in a fairly large (unconfined) channel; for $\delta > 0.8$, the wall had a negligible effect on the flow, but asymmetric flows were observed for $0.3 < \delta < 0.6$. For $\delta < 0.3$, the shear layer close to the wall remained steady and did not curl up into a discrete vortex, thus suppressing vortex-shedding, similar to the findings of Lei et al. [31]. The flow patterns for $\delta = 0.1$ and 0.2, when the cylinder was very close to the wall, were different; for $\delta = 0.1$, no periodicity was found in either shear layer, while for $\delta = 0.2$, the shear layer near the wall was steady, and the layer near the freestream exhibited periodicity. Due to the flow confinement experienced in micromixers with obstacles, offsetting the latter from the channel centreline, can yield small gap ratio values which, as highlighted by

the work of Wang and Tan [33] and others, can have a very complex effect on the flow and mixing.

In light of the above, the aim of this work is to experimentally investigate the effects of obstacle and fluid interface offset on the flow and mixing performance, addressing thus some of the outstanding questions outlined previously. In particular, it remains to be explored whether offsetting a cylindrical obstacle (micropin) toward the fluid interface can enhance mixing, i.e. will it facilitate faster diffusion by increasing the interfacial area of the fluid streams, or will it hinder mixing because the small gap ratio suppresses vortex-shedding? Micro particle-image velocimetry (µPIV) and micro laser-induced fluorescence (µLIF) are employed to measure the instantaneous velocity and concentration fields respectively, in the flow past a confined microfluidic cylindrical pin placed in a Y micromixer with a fixed level of confinement and varying offset pin and interface positions. The wake characteristics and corresponding mixing indices are determined from the acquired data for a range of flow conditions and various mixing mechanisms identified.

2. Experimental set-up

2.1. Microfluidic chip fabrication

Polymethyl methacrylate (PMMA) rectangular microfluidic channels with a Y-junction inlet geometry and a single cylindrical pin located at different offset positions from the centreline were fabricated using CNC micro-milling (Minitech Machinery, Georgia) and bonded using a solvothermal bonding technique [34]. The diameter (D) of the cylindrical pin was equal to 530 ± 10 µm, the channel height (H) 1000 ± 10 µm and

the width (W) 1480 ± 10 μm, resulting in a vertical confinement of $h^* = 1.9$ and a lateral confinement of $w^* = 2.8$.

A schematic of the Y-microchannel is shown in Fig 1. The inlet angle (θ) was kept small (6 ± 1°) to minimize separation effects and achieve fully developed flow upstream of the pin. This ensured that the observed mixing enhancement was due to the pin itself rather than the Y-inlet as demonstrated in previous studies [35,36]. The interface position (l/W) and gap ratio ($\delta = g/D$), defined in Fig. 1, are the two of the key parameters varied in this study. Two interface positions were considered: $l/W =$ 0.5 and 0.3 respectively. In the former, the fluid interface is aligned with the microchannel centreline whereas in the latter it is offset to a location that is a third of the channel width by pumping the fluids to be mixed at a flow rate ratio of 1:2. The pin location was also varied resulting in gap ratios of 0.19, 0.42 and 0.89. Note that $\delta =$ 0.89 corresponds to the pin positioned on the centreline (i.e. a symmetric channel). The total channel length was 120 mm and the distance from the inlet to the micropin was 50 mm, i.e. 94 D, which is sufficient to ensure a fully developed flow upstream of the pin. Two channels with $l/W =$ 0.5 and 0.3 without a cylindrical pin were also fabricated and used as reference channels.
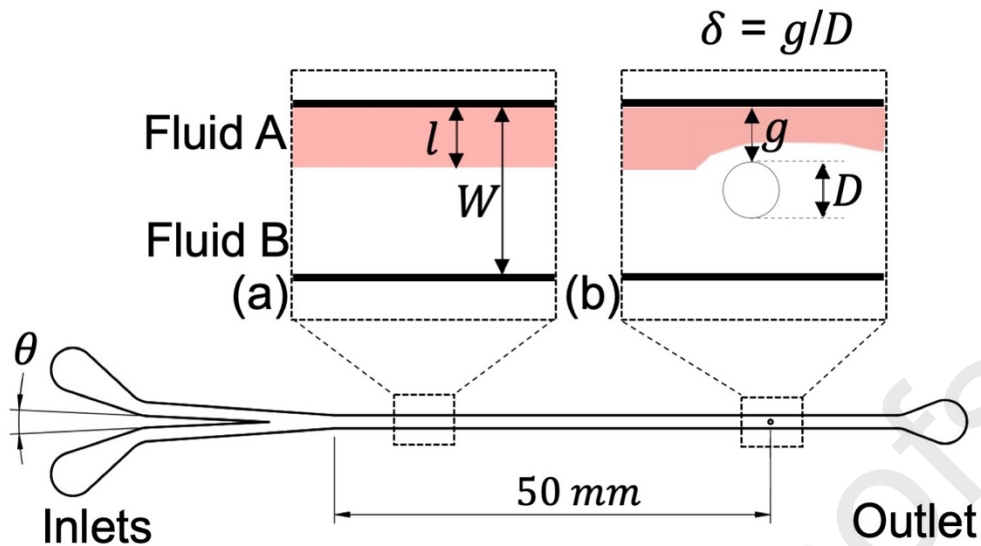
Fig. 1. Schematic of the microfluidic channels with a single cylindrical pin, showing the angle between the two inlets (θ) as well as the definitions of the initial position of the fluid interface (l/W) and gap ratio ($\delta = g/D$).

2.2. Micro particle-image velocimetry (μPIV) system

The micro particle-image velocimetry system used in the present study is shown in Fig. 2. It comprised a pulsed Nd-YAG laser with a wavelength of 532 nm (Litron Laser, UK), a bespoke microscope assembly (Edmund Optics, UK) and a scientific complementary metal-oxide-semiconductor (sCMOS) camera (Zyla 5.5, Andor, UK). The microfluidic chips were mounted on a three-axis motorized translation stage (Thorlabs, UK). Distilled water was used as the working fluid at room temperature. The flow was seeded with 1 μm neutrally buoyant Nile Red fluorescent polystyrene particles (ThermoFisher, UK) and was driven by two syringe pumps (Harvard Bioscience, USA) at flow rates ranging from 0.2 to 105 ml/min with ± 1 % accuracy. μPIV measurements were taken at various planes along the span of the cylinder with the majority at the mid span. A 5x microscope objective (Numerical Aperture of 0.14) was used resulting in an in-plane spatial resolution

of 1.33 µm/pixel and the maximum image size was 2560 × 2160 pixels. In each experiment, 100 image-pairs were acquired at a framerate of 15 Hz and processed using a multi-pass cross-correlation procedure with a 50% window overlap (Insight4G, TSI, USA), starting with an interrogation window of 128 × 128 pixels and ending with 64 × 64 pixels.

In the present µPIV setup, the measurement volume thickness, given by the depth of correlation [37], was estimated to be around 120 µm. It is well documented in the literature that the velocities measured by µPIV systems are affected by errors arising from the depth of correlation [38], leading to underestimates of up to a factor of 2/3 [39]. Such systematic errors are integral to µPIV measurements, and hence the depth of correlation is not expected to have considerable influence in the overall accuracy of the in-plane results. To eliminate the need to correct the measured data [39] and facilitate comparisons between the cases studied, all reported velocity measurements are normalized by the average velocity U_o determined from the measured velocity profiles upstream of the pin.
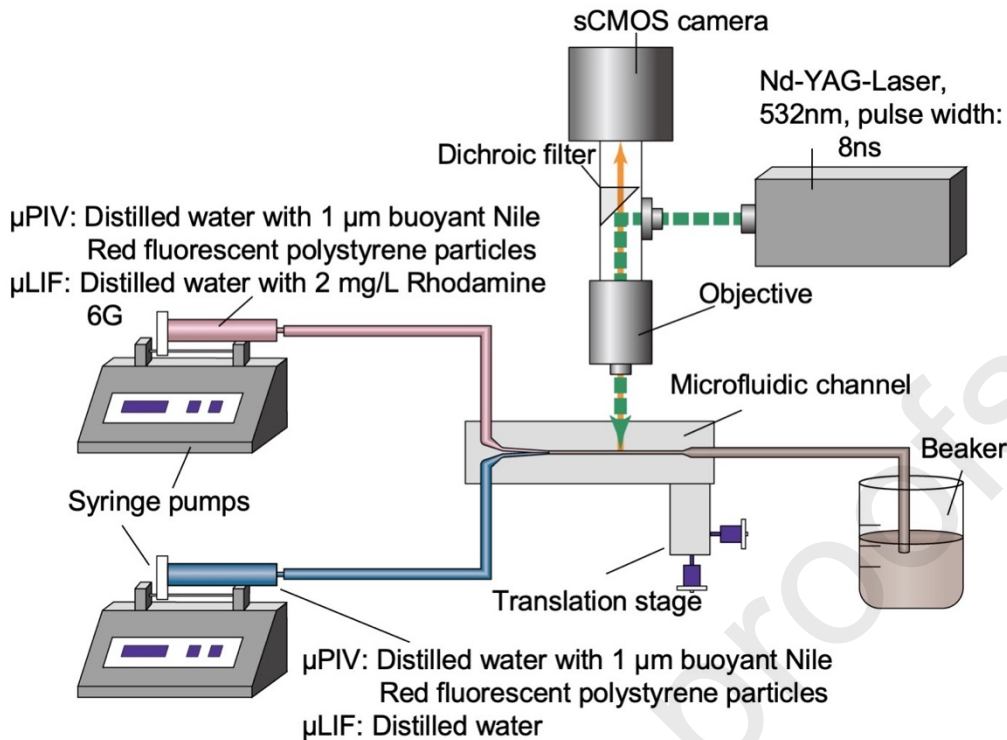
Fig. 2. Schematic of the experimental setup employed for µPIV and µLIF measurements.

2.3. Micro laser-induced fluorescence (µLIF) system

The setup described above was also utilized for the µLIF measurements, with the laser emitting single rather than double pulses with a pulse duration of 8 ns. An aqueous solution of the fluorescent dye Rhodamine 6G (Sigma-Aldrich, UK) was perfused through one of the inlets of the channel. Rhodamine 6G has a maximum absorption wavelength of 530 nm, a maximum emission wavelength of 560 nm and very little temperature or pH sensitivity [19], and so was well-suited for these measurements. Figure 3 shows the calibration curve. In a reference microchannel (without cylindrical pins), the sCMOS camera was used to capture the fluorescence intensity while varying the concentrations of the dye (ranging from 0.25 mg/L to 16 mg/L). The results are shown in Fig. 3a (in which the intensity value was found by averaging over the whole image before normalization); the fluorescence intensity variation is found to be linear

in the low concentration regime (Fig. 3b). The linear regression line in Fig. 3b has a R-squared value of 0.996. Therefore, the concentration of Rhodamine 6G in one inlet stream, c_o, was chosen to be 2 mg/L in all experiments. In each experiment, the channel was perfused with pure water and Rhodamine 6G solutions to obtain reference images for the minimum (0 mg/L) and maximum (2 mg/L) Rhodamine 6G concentrations. Afterwards, 100 images were acquired with a frame rate of 15Hz and image background-subtraction and intensity normalization steps were implemented using Matlab (the process is shown in the Supplementary Material 1).
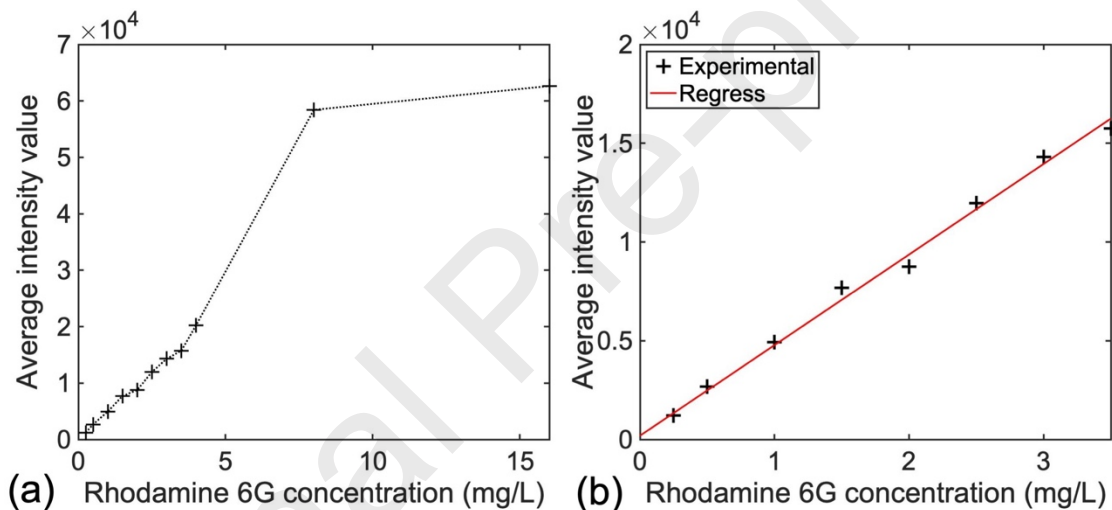

Fig. 3. The relationship between fluorescence intensity and concentration of Rhodamine 6G in a reference microchannel. Black cross symbols are experimental data (a) ranging from 0 to 16 mg/L and (b) ranging from 0 to 3.5 mg/L. The red solid line is the regression line of experimental data with a R-squared value of 0.996.

3. Results and discussion

3.1. Upstream flow characterization

Prior to the analysis of mixing, the upstream flow was characterized at the chosen operating conditions. This process involved determining whether the upstream flow is

fully developed, and estimation of the average flow velocity. Velocity measurements were taken at different spanwise planes and compared with the analytical solution for fully developed, three dimensional laminar flow in a rectangular channel [40] given by:

$$U_x(y,z) = \frac{4H^2 \Delta p}{\pi^3 \eta L} \sum_{n,odd}^{\infty} \frac{1}{n^3} \left[1 - \frac{\cosh\left(n\pi\frac{y}{H}\right)}{\cosh\left(n\pi\frac{w}{2H}\right)} \right] \sin\left(n\pi\frac{z}{H}\right), \qquad (3)$$

where Δp is the pressure drop along the channel and η is the dynamic viscosity [40]. Fig. 4 shows a comparison between the velocity measurements and the analytical solution at the highest flow rate measured in a microchannel with δ = 0.89 and l/W = 0.5. The experimental data were acquired at x/D = -10 (i.e. 10D upstream of the centre of the cylindrical pin) and at different z planes in the range z/D = -0.95 to 0.95 which were combined to obtain the 3D flow velocity upstream of the micropin. These 3D velocity profiles were used to calculate the average velocity of the approaching flow U_0 as well as the Reynolds number. The uncertainty in the PIV measurements was estimated using the difference between the primary and secondary peak in the cross-correlation matrices [41] and was found to be 2%. Based on the channel geometries, the uncertainty in channel dimensions was around 1%. With room temperature varying between 17 ℃ and 20 ℃, the resulting uncertainty in viscosity is around 4%. From error propagation we can estimate the error in the Reynolds number to be around 5%. Selected upstream velocity profiles measured for different values of δ and l/W at the channel midplane (z/D = 0) at the highest examined Re are also compared against the analytical solution in Fig. 5. Excellent agreement with the analytical solution (within 4%) can be observed, confirming that the flow approaching the pin is fully developed. To ascertain the nature of the microchannel flow, Re is also calculated based on the hydraulic diameter of the microchannel. The range of examined Re is between 81 to 726 (corresponding to Reynolds numbers based on pin diameter of 33 to 298), which belongs to the laminar flow regime.
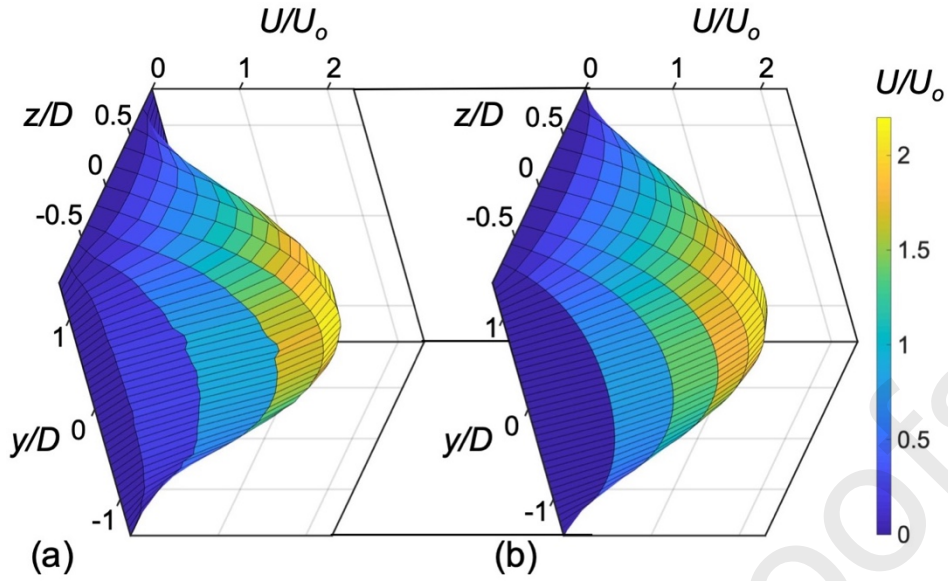
Fig. 4. (a)Three-dimensional velocity measurements of the flow approaching the micropin and (b) the analytical solution in a microchannel with δ = 0.89 and l/W = 0.5 at Re = 678. Velocities are normalized with the average velocity U_0 obtained from the PIV measurements.
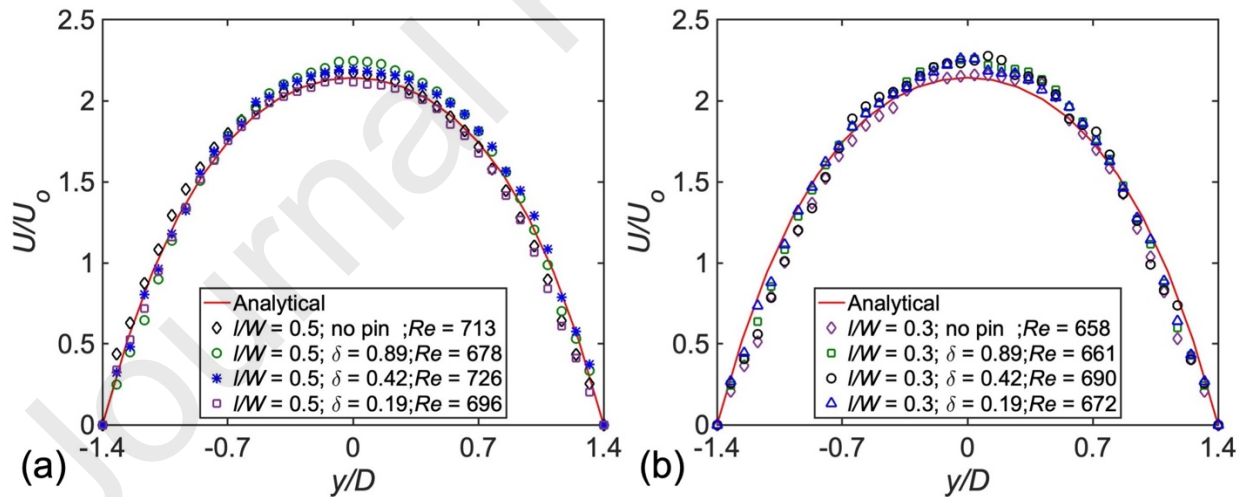

Fig. 5. Comparisons between experimental data with (a) l/W = 0.5 and (b) l/W = 0.3 as well as analytical (solid line) velocity profiles upstream of the micropin (x/D = -10, z/D = 0) for various values of gap ratio δ and Reynolds numbers.

3.2. Velocity and concentration fields in the pin near wake

In order to investigate the effects of gap ratio and the position of fluid interface on mixing performance, the flow and concentration fields in the near wake of the pin were characterized at the channel midplane (z/D = 0) for Re in the range between 170 and 186, as shown in Fig. 6. This Re number is below the critical one for the onset of vortex-shedding [11] and hence the flow fields in Fig. 6 are steady. In the channel without the cylindrical pin (top row), the streamlines are uniform and parallel (Fig. 6a), and mixing is diffusion-dominated. The average flow velocity is around 0.15 m/s at $Re \approx$ 180, resulting in a residence time of 0.33 s from the inlets to the pin location. The diffusion coefficient value of Rhodamine 6G in water at 25 °C is 4.14 × 10-6 cm2/s [42]. Therefore, the fluorescent dye crosses the fluid interface by diffusion by about 11.7 μm in the transverse direction (0.8% of the channel width), indicating that the diffusive mixing is relatively weak. This is evident in the sharpness of the fluid interface in the instantaneous concentration fields (Fig. 6e and 6i).

In the channel with the pin and fluid interface both located at the channel centreline (δ = 0.89, l/W = 0.5), a pair of vortices can be seen downstream of the pin (see Fig. 6b), promoting mixing in the near wake region (Fig. 6f). However, Fig. 6j indicates that when the fluid interface is off the centreline (l/W = 0.3), the dye does not become entrained into the wake and mixing is limited. When the pin is offset such as δ = 0.42, a pair of asymmetric vortices that remain attached to the cylinder are formed, as can be seen in Fig. 6c. Offsetting the pin only results in the near wake being composed entirely of fluid from the upper fluid layer (i.e. the dyed layer, with c/c_o = 1), with little enhancement of mixing (Fig 6g). On the contrary, when the fluid interface is also offset by a similar amount from the centreline, i.e. coincides with the axis of the pin (l/W = 0.3, Fig. 6k), fluid from both fluid layers becomes entrained in the wake and thus acts

to promote mixing. Finally, when the gap ratio reduces to δ = 0.19, a vortex forms at the channel wall (Fig. 6d), deflecting the flow around the pin and causing the interface between the fluid layers to also be deflected away from its upstream position (i.e. y/D = 0), before reverting to this position downstream (Fig. 6h). Similar trends can also be seen in Fig. 6l for l/W = 0.3. Despite the shifting of the fluid interface closer to the pin location, no significant effect on mixing can be achieved as the pin still remains immersed in one of the fluid layers, unable to entrain fluid from the non-dyed stream.

The effects of the cylinder on the mixing performance are considerably different when the Reynolds number exceeds the critical value for the onset of vortex-shedding; this was found to be at Re = 440 for the microchannel with the pin located on the centreline (Zhang et al. 2019). Fig. 7 shows selected instantaneous velocity and concentration fields for Re in the range between 509 and 546. Vortex-shedding can clearly be seen in both the flow and concentration fields obtained with the pin located on the centreline (second row of Fig. 7), leading to a strong enhancement of mixing. The near wake in Fig. 7f is now characterised not by a narrow interface between blue and yellow regions ($c/c_o \approx 0$ and ≈ 1, respectively), but by a relatively broad region of well mixed fluid ($c/c_o \approx 0.5$). Vortex-shedding also distorts the fluid interface for the l/W = 0.3 case (Fig. 7j), but fails to promote mixing in the wake. Clearly, with higher Re, offsetting the pin towards the channel wall results in slightly different flow patterns compared to those obtained with Re = 180, characterised by a longer wake region for the case with δ = 0.42 (Fig.7c), and the formation of two vortices in the smaller gap ratio case (δ = 0.19, Fig. 7d); one at the channel wall ($x/D \approx 3$) and one at the pin. However, the concentration fields measured for l/W = 0.5 (Figs. 7g, h) are not significantly altered by the increase in Re due to the formed vortices remaining within a single fluid layer

and hence not promoting significant advective mixing. This could indicate the absence of vortex-shedding in these two cases as the proximity of the sidewalls is expected to shift the flow separation point further downstream, and inhibit vortex-shedding [32].

The results in Fig. 7 also show that when the interface of the two fluids to be mixed coincides with the axis of the pin, mixing is promoted in the near wake. This is evident in the case of l/W = 0.5 and the pin located at the channel centreline (δ = 0.89) as well as in the case of l/W = 0.3 and δ = 0.42 (Figs. 7f, k). Offsetting the cylindrical pin from the channel centreline and toward the fluids interface position l/W = 0.3 has a destabilizing effect on the fluid interface, which in turn promotes near wake mixing, despite the suppression of the onset of vortex-shedding by the wall proximity. The vortex forming at the channel wall for δ = 0.19 has no effect on mixing as it cannot disrupt the interface between the two fluids located further from the wake.

Videos of velocity fields and concentration fields of l/W = 0.5 and 0.3 corresponding to Fig. 6 and Fig. 7 can be found in Supplementary Videos 1 and 2. Supplementary Video 3 presents the velocity fields and concentration fields of l/W = 0.5 and 0.3 at the highest Re range examined (678 < Re < 726) in the present study.
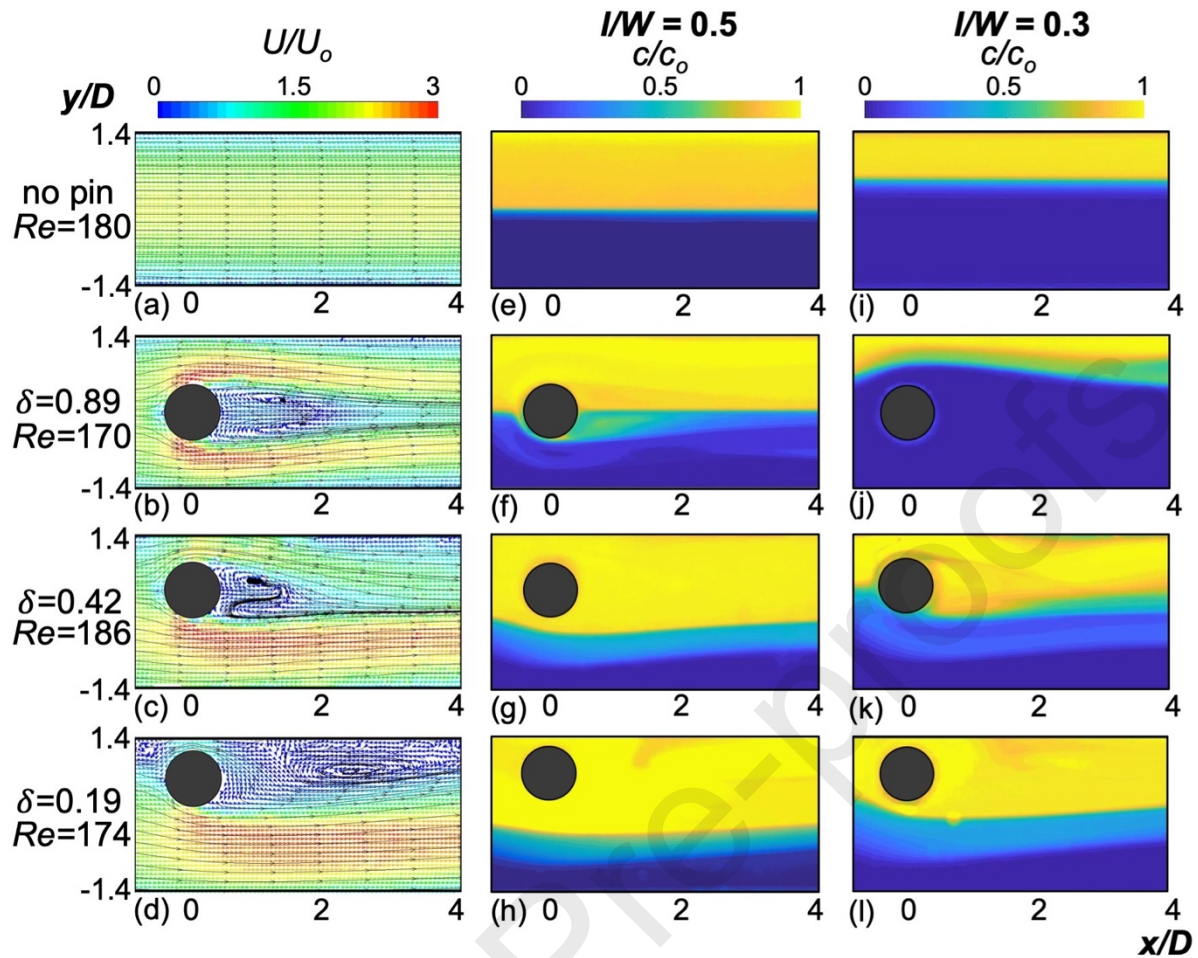
Fig. 6. Instantaneous velocity fields with superimposed streamlines (left column) and instantaneous concentration fields (middle and right columns), for channels with the fluids interface located at the centre of the channel (*l/W* = 0.5, middle column) and offset (*l/W* = 0.3, right column) for different gap ratios. The Reynolds number ranges from 170 to 186, and the flow is steady in each case.
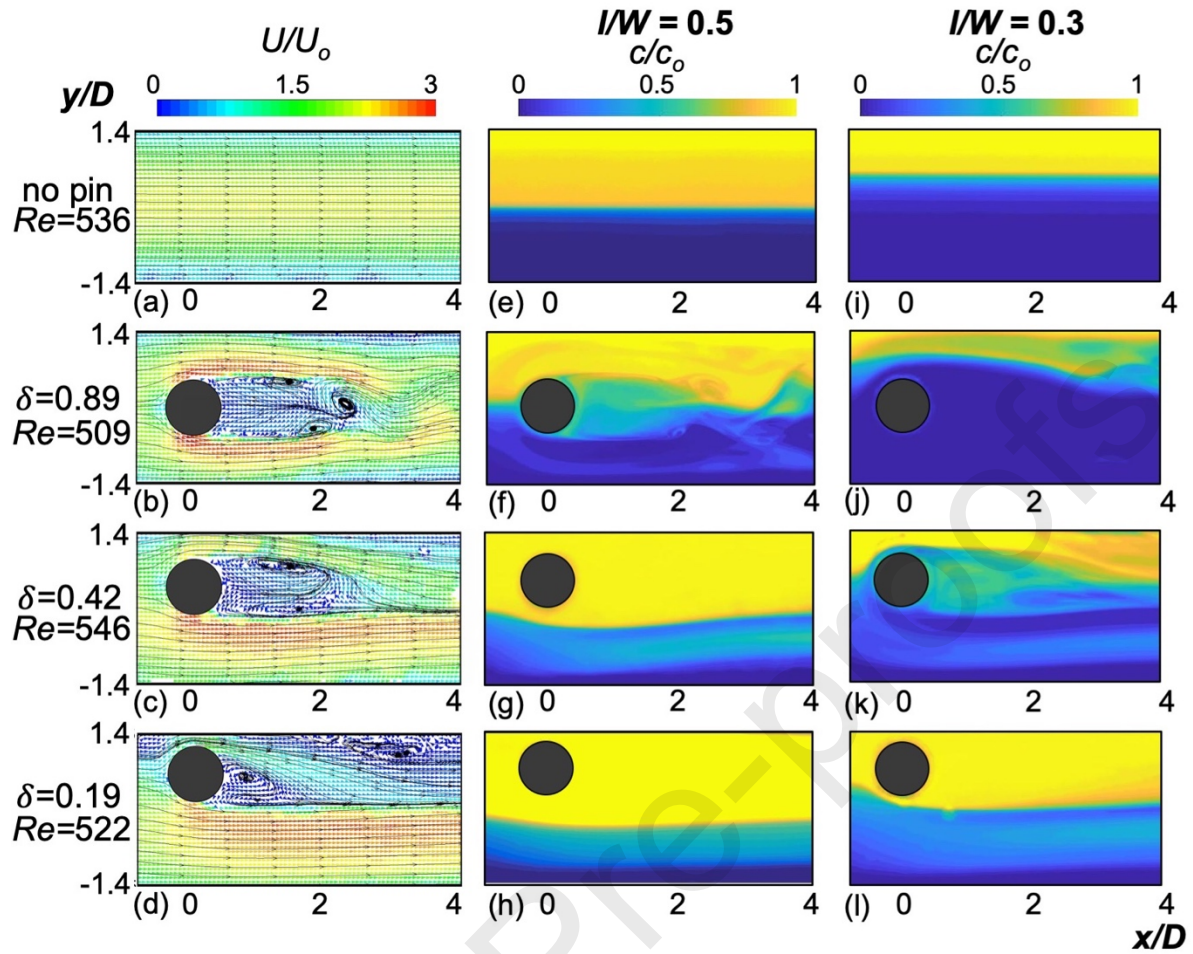
Fig. 7. Instantaneous velocity fields with superimposed streamlines (left column) and instantaneous concentration fields (middle and right columns), for channels with the fluids interface located at the centre of the channel ($l/W = 0.5$, middle column) and offset ($l/W = 0.3$, right column) for varying gap ratio. The Reynolds number ranges from 509 to 546.

3.3. Mixing characterization for l/W = 0.5

In order to fully understand the effect of the pin on the fluid mixing outside of the near wake region and to assess the overall performance of the micromixer, further concentration measurements were acquired both several diameters upstream and downstream of the pin location. Figs. 8 and 9 show instantaneous concentration fields acquired upstream, in the near wake and the far wake for l/W =0.5 with Re in the

ranges of 340 to 366 and 678 to 726, respectively. For the cases without a pin (top row in both figures), the concentration fields are essentially identical upstream ($x/D \approx$ -8) and downstream ($x/D \approx$ 12), since lateral diffusion is slow compared to the flow velocity, indicating that any significant changes in the concentration fields occur as a result of the presence of the pin. None of the concentration fields in Fig. 8 show signs of vortex-shedding (although symmetric, attached vortices can be seen in Fig. 8f), because the Reynolds number is relatively low. Nevertheless, even in the absence of vortex-shedding, the presence of the pin causes a significant enhancement in fluid mixing downstream at $x/D \approx$ 12 (right column in Fig. 8). This is most clearly seen when the cylinder is offset from the centreline and is also apparent slightly upstream of the cylinder. Given the weak role of diffusion, the enhancement of steady-state mixing is most likely a result of the development of three-dimensional flow structures in the flow near the cylinder [43].

In the instantaneous concentration fields at higher Re (ranging from 678 to 726), unsteady flows can be observed downstream of the pin as shown in the right column of Fig. 9. In this case, the far wake region for δ = 0.89 (Fig. 9j) is highly disordered, showing strong mixing throughout the channel width. There is also enhanced mixing for the offset pin locations in the far wake (Fig. 9k and 9l) compared to the corresponding steady-state cases in Fig. 8, but the improvement is not as pronounced.
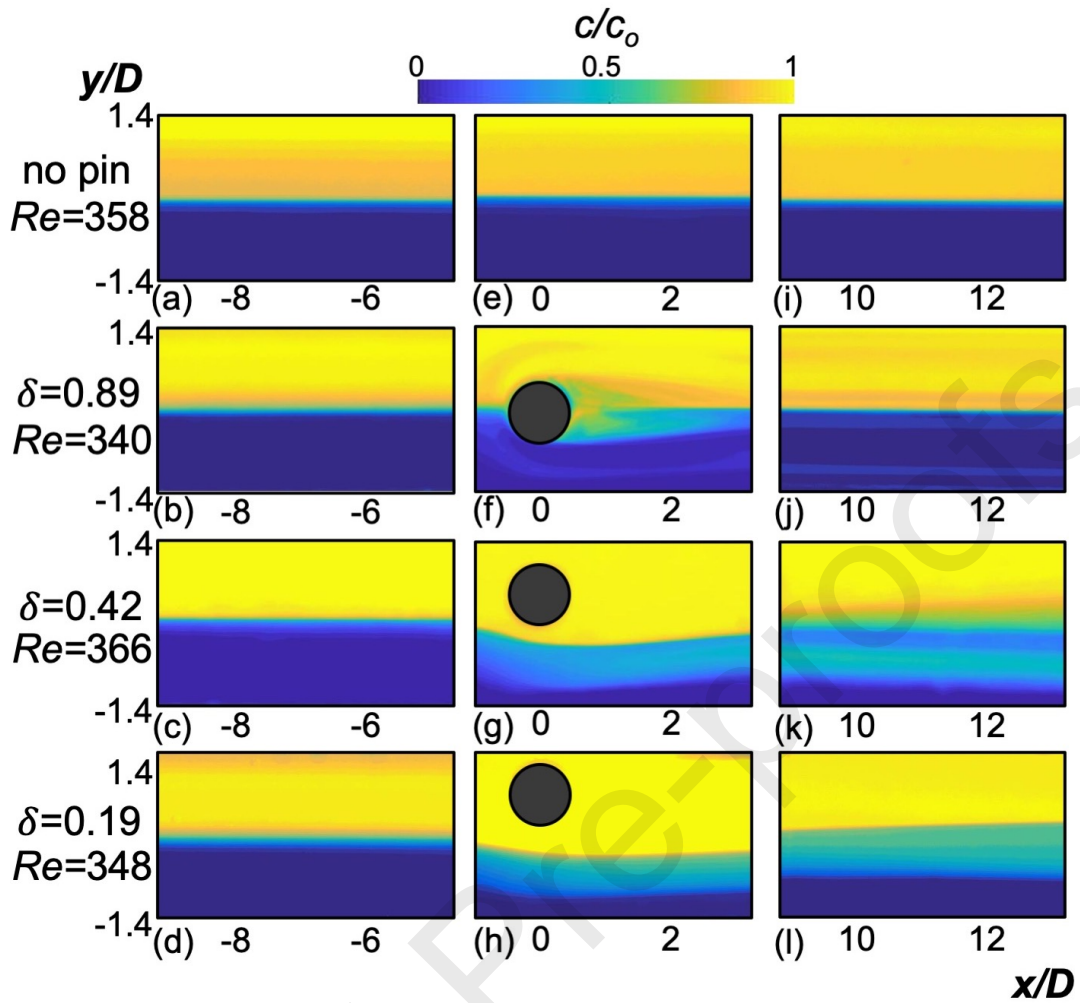
Fig. 8. Instantaneous normalized concentration fields in the flow region ranging from -9 < *x/D* < 13, with the position of fluids interface set to *l/W* = 0.5 and various gap ratios. The Reynolds number ranges from 340 to 366 and the flow is steady, i.e. there is no vortex-shedding.
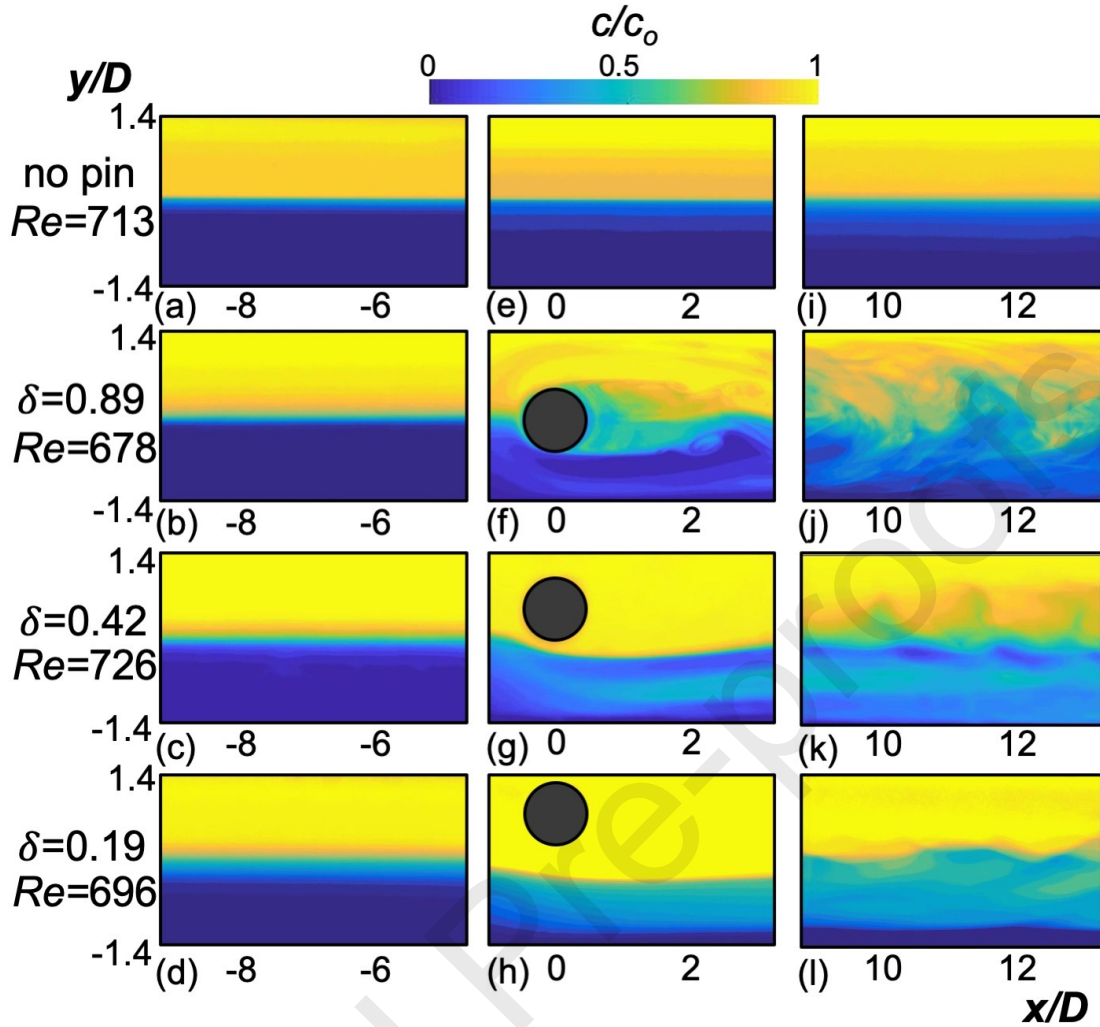
22

Fig. 9. Instantaneous normalized concentration fields in the flow region ranging from -9 < *x/D* < 13, with the position of fluids interface set to *l/W* = 0.5 and various gap ratios. The Reynolds number ranges from 678 to 726, i.e. above the critical *Re* for the onset of vortex-shedding in a channel with similar dimensions and a pin located on the centreline.

In order to quantify the effect of the pin location on the mixing process described above, the intensity of segregation technique (Eq. 1 and 2) was applied to the LIF data. The mixing index was estimated as a function of *x/D* by dividing each concentration field into strips, 20-pixels in width, and calculating the mean and standard deviation of the intensity in each strip over 100 instantaneous images. The number of pixels of each

strip was chosen to ensure that the estimates of $\bar{c}$ and σ_c were robust (i.e. the sample size was sufficiently large to achieve convergence) and that the profiles of M were not significantly affected by noise in the concentration field measurements. The detailed validations are shown in the Supplementary Materials 2 and 3. Note that the value of M was estimated based on the concentration fields obtained at the channel mid-plane (z/D = 0), which is considered as a representative indication of mixing in a specific cross-section within the microchannel (i.e. for a specific x/D). It is plausible that the M for a cross-section will be influenced by the 3D nature of the confined flows that are not captured here [11]; hence, strictly speaking, M values reported here should be considered limited to a line in the plane of the μLIF measurements. The error bars indicate the standard deviation of M evaluated from the number of experimental images used in the averaging (100 images in each case).

The variation in the mixing index M with streamwise position x/D is shown in Fig. 10 for the various pin offset cases corresponding to the data sets presented in Figs. 8 and 9. Upstream of the pin, in the region x/D = -10 to -4, the mixing performance of all cases is relatively low ($M \approx 10\%$). This is the same regardless of whether a pin is present or not, and therefore the non-zero value of M is likely to be the result of diffusion, experimental error and the minor unavoidable level of mixing at the inlet where the two fluid layers first come into contact. For the channel without a pin, the inhomogeneity of the flow remains relatively constant over the entire region examined, as expected. For most other cases in Fig. 10a, there is an increase in M near x/D = 0, even in the absence of vortex-shedding, which may be attributed to the entrainment of fluids from both layers into the recirculation bubble, which then acts as a mixer. For δ = 0.89, M reverts to its upstream value of approximately 10% by $x/D \approx 5$ (i.e. by the

end of the recirculation bubble), while for the offset pins, the mixing index remains relatively high (>20%) further downstream. In a symmetric channel with steady flow, the three-dimensional flow features will also be symmetric [43], and they do not lead to an increase in mixing when the interface lies at the centreline (i.e. the line of symmetry). Also, there is no instability to introduce interface waviness that can propagate downstream at this relatively low Re. It can therefore be concluded that when the fluid interface lies at the centreline of the channel, in the absence of vortex-shedding, asymmetrically positioned pins are a more effective means of promoting mixing.

When vortex-shedding occurs (Fig. 10b), the mixing index also increases near x/D = 0. However, in this case, the periodic flow in the wake ensures that M values remain large downstream. In contrast to the pre-vortex-shedding case, the mixing index in the far wake decreases as the pin is offset from the centreline, indicating that vortex-shedding is more effective in promoting mixing compared to pin location. The strongest mixing enhancement is achieved when the pin axis coincides with the fluid interface (l/W = 0.5 in this case), i.e. δ = 0.89.
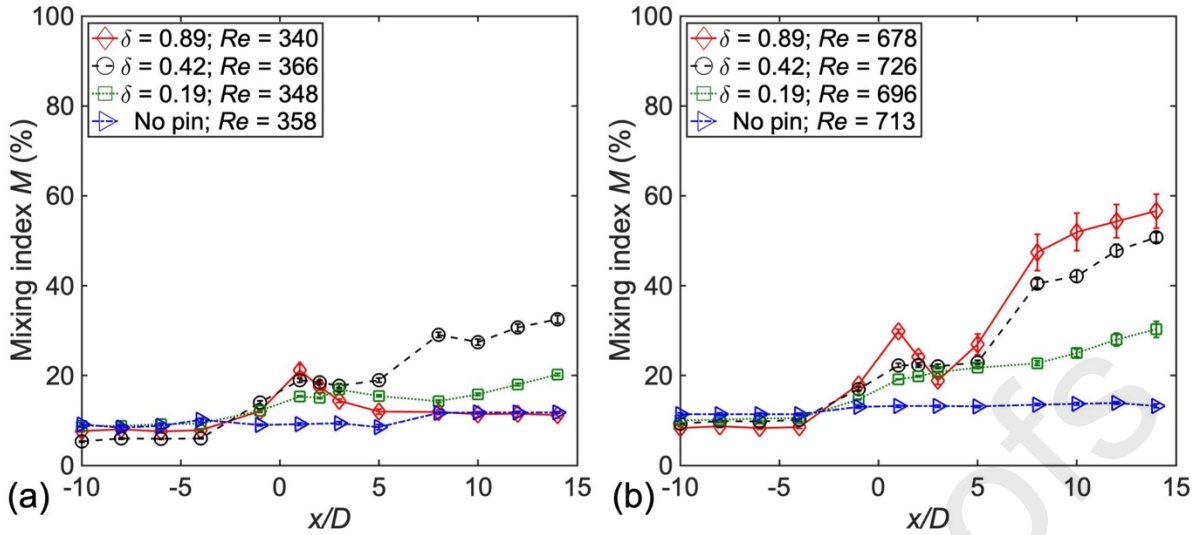
Fig. 10. The variation of the mixing index M along the channel (x/D = -10 to 14) for l/W = 0.5 and various δ and Re (cases shown in Fig. 8 and Fig. 9). (a) Re ranging from 340 to 366 (pre-vortex-shedding) and (b) Re ranging from 678 to 726 (with vortex-shedding). Note that some of the symbols are larger than the error bars.

3.4. Mixing characterization for l/W = 0.3

Selected instantaneous normalized concentration fields measured upstream, in the near and far wake of the pin are shown in Fig. 11 for the cases in which the fluid interface is offset from the channel centreline (l/W = 0.3) and for Re in the range of 328 to 343. The upstream concentration fields (left column) are similar in all cases, regardless of whether a pin is present. Therefore, the values of M would be expected to be similar and low in this region. In the channel without a pin (top row), as noted in the previous section, the concentration fields do not show any significant change from x/D = -9 to 13, and so any mixing enhancements in other channels can be attributed to the presence of pins. When the pin is located at the centreline (δ = 0.89, Fig. 11f), it causes the fluid interface to shift towards the wall, before reverting back towards its original position downstream. This deformation of the interface (and potential three-dimensional effects)

26

result in improved diffusive-mixing. Further evidence of three-dimensionality in the flow can be seen in the downstream concentration field (Fig. 11j), in which the dye concentration appears weakened close to the wall (y/D > 1), but remains relatively strong near y/D = 0.5. The non-monotonic relationship between c and y/D at this downstream location cannot be attributed to diffusion (as diffusive processes cannot cause a monotonic profile to become non-monotonic), but can be explained by the development of streamwise vortices near the ends of the cylinder, i.e. swirling flow [43]. Similar evidence of potential three dimensionality effects can be seen in the downstream fields for δ = 0.42 and 0.19 (Fig. 11k and 11l, respectively), where the concentration varies considerably with y/D. The non-monotonic variation in concentration distribution is not as evident when the fluid interface is located at the centreline, i.e. $l/W = 0.5$ (since the three-dimensional flow is itself symmetric about y/D = 0), suggesting that flow three-dimensionality is more effective at producing mixing when the interface is offset.

The corresponding concentration fields at Re in the range of 658 to 690, i.e. above the critical Re for the onset of vortex-shedding, are shown in Fig. 12. For δ = 0.89, the asymmetry of the fluid streams means that the near wake of the cylinder is composed mostly of pure water (blue region in Fig. 12f). Vortex-shedding enhances chaotic advection and there is greater mixing in the far wake (Fig. 12j), although not much dye has crossed the channel centreline. In the channel with δ = 0.42, where the fluid interface upstream coincides with the pin axis (Fig. 12 g, k), good mixing can be observed in both the near and far wake. Offsetting the pin closer to the wall (δ = 0.19), mostly enhances the dispersal of dye throughout the channel. The data in Fig. 12 clearly demonstrate that when the interface between the two fluids does not lie at the

centre of the channel, the pin is much more effective at dispersing the fluid layers if it is positioned away from the centreline and closer to the interface.

Note that sample videos of the concentration fields with $l/W = 0.5$ at Re of ranging from 509 to 546 and $l/W = 0.3$ at Re ranging from 497 to 518 are shown in the Supplementary Videos 4 and 5.
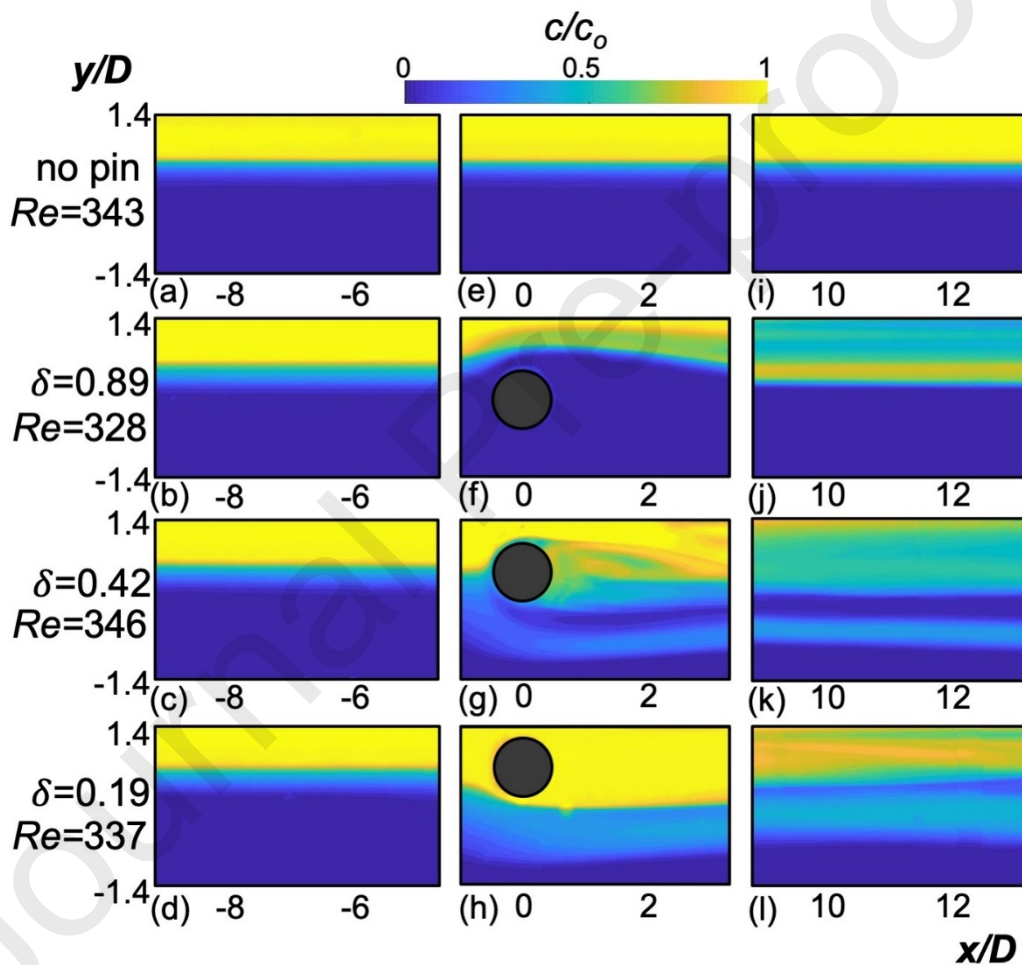

Fig. 11. Instantaneous normalized concentration fields in the flow region ranging from $-9 < x/D < 13$, with the position of the fluids interface set to $l/W = 0.3$ and various gap ratios. The Reynolds number ranges from 328 to 346 and the flow is steady, i.e. there is no vortex-shedding.
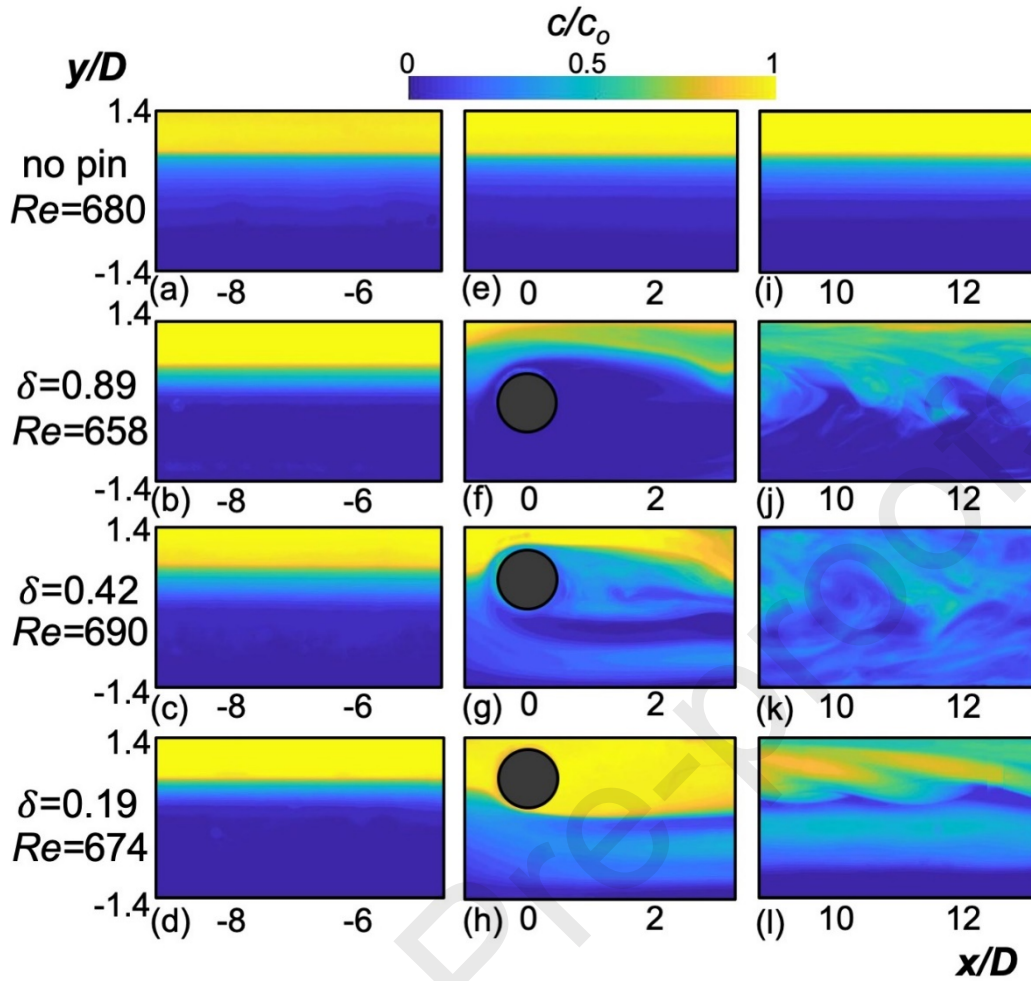
Fig. 12. Instantaneous normalized concentration fields in the flow region ranging from -9 < *x/D* < 13, with the position of the fluids interface set to *l/W* = 0.3 and various gap ratios. The Reynolds number ranges from 658 to 690, i.e. above the critical *Re* for the onset of vortex-shedding in a channel with similar dimensions and a pin located on the centreline.

The variation in the mixing index with *x/D* is shown in Fig. 13 for *Re* in the range of 328 to 346 and 658 to 690 (corresponding to Fig. 11 and Fig.12). In the channel without a pin (blue lines in Fig. 13), *M* is again roughly constant over the range *x/D* = -10 to 14. As noted in the previous section, there is a sudden increase in *M* near *x/D* = 0. Before the onset of vortex-shedding, there is a non-monotonic relationship between δ and the

far wake values of M in both l/W cases (0.5 and 0.3), with the optimal values obtained with the pin offset at δ = 0.42 (see Figs. 10a and 13a). At higher Re, the most effective mixing occurred for δ = 0.42 at l/W = 0.3 as it coincides with the interface location (black line in Fig. 13b). Similar trends are observed at l/W = 0.5 with the cylindrical pin aligned with the fluid interface. Similar mixing index values can be found for the δ = 0.19 and 0.89 channels.
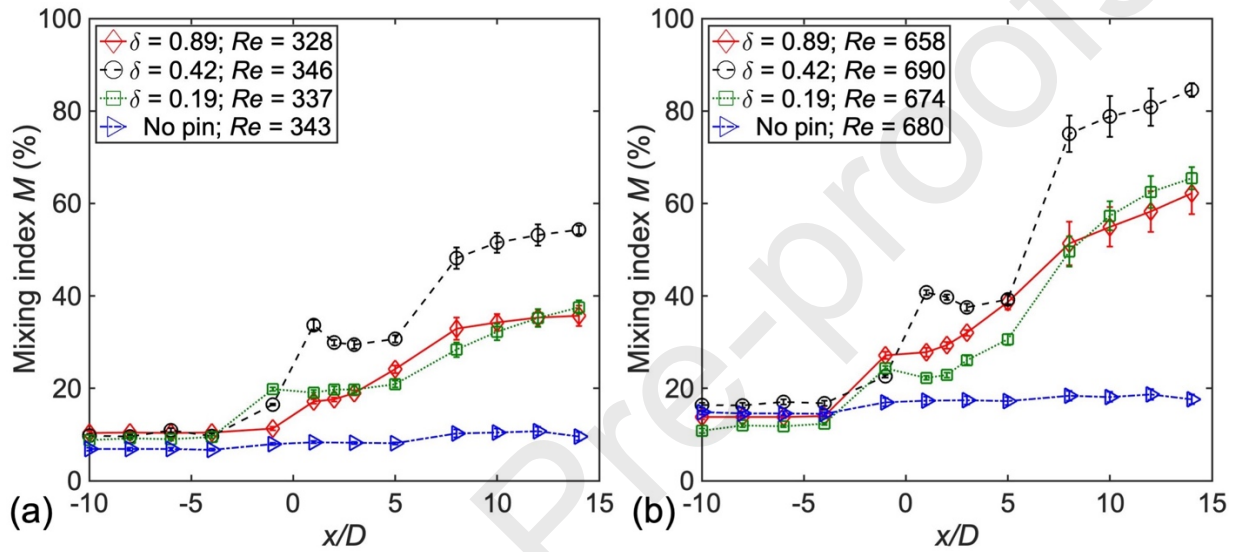

Fig. 13. The variation of the mixing index M along the channel (x/D = -10 to 14) for l/W = 0.3 and various δ and Re (cases shown in Figs. 11 and 12). (a) Re around 350 (pre-vortex-shedding) and (b) Re around 700 (with vortex-shedding). Note that some of the symbols are larger than the error bars.

In order to compare the mixing performance in channels with different Reynolds number, the relationship between Re and mixing index at a specific streamwise location, x/D = 12, is shown in Fig. 14 for two different fluid interface positions. In channels with no pin, M is always low (less than 15%) with Re ranging from 100 to 700. Therefore, the present study indicates that the effect of the fluid interface position on mixing is negligible in the absence of a pin for 100 < Re < 700. This appears to be

in agreement with published numerical work [29] that reported a significant effect of the interface position (*l/W*) on microchannel mixing for *Re* < 0.1, i.e. when mixing is dominated by diffusion, but a negligible one for higher *Re* values (ref. [29] considered *Re* ranging from 5 to 10 to infer this).

The difference introduced by the presence of the pin is also very clear from Fig. 14. When *l/W* = 0.5, i.e. the two fluids are mixed at the same ratio (Fig 14a), the presence of a pin at the channel centreline (δ = 0.89) does not dramatically enhance mixing further downstream prior to the onset of vortex-shedding (at around *Re* of 440). While there has been significant interest in the performance of micromixers at low *Re* [10,21,27], the sudden increase in *M* near the critical Reynolds number indicates that there is great potential to further enhance mixing by raising *Re* sufficiently high to induce unsteady flow. When *l/W* = 0.3, i.e. the two fluids are mixed at a 1:2 ratio, a pin located on the channel centreline (δ = 0.89) can improve the mixing performance downstream in the absence of vortex-shedding (see red dashed line in Fig. 14b); this is due to the pin disturbing the fluid interface, which can increase lateral concentration gradients and thus enhance diffusive mixing; it also appears to induce some transverse flow, which promotes convective mixing (see Fig. 6b and Fig. 6j). The mixing performance with *l/W* = 0.3 and δ = 0.89 increases in a roughly steady manner with *Re*, even as the flow transitions from the steady to the unsteady regime. When vortex-shedding is present (*Re* > ~ 440), the mixing index is similar regardless of the position of the interface (for *l/W* = 0.3 and 0.5) for δ = 0.89.

The largest mixing enhancement downstream is seen for the δ = 0.42 microchannel. For *l/W* = 0.5, *M* increases with *Re*, but interestingly, it does not exhibit a jump at the

onset of vortex-shedding (Fig. 14a), unlike that seen for the symmetric microchannel geometry (δ = 0.89). Interestingly, when the fluid interface is offset (l/W = 0.3), the onset of vortex-shedding coincides with a clear drop in M (Fig. 14b). The values of M in this local minima are comparable to those seen in the same Re range for l/W = 0.5, suggesting that the reduction in M near the critical Reynolds number occurs because mixing due to unsteady vortex-shedding is less efficient than the steady mixing due to the three-dimensional flow features at slightly lower Re. A small decrease in M can also be seen for l/W = 0.3 and δ = 0.89, highlighting the sensitivity of the micromixer performance to the interface position.

For the microchannel with the greatest pin offset (δ = 0.19), mixing is enhanced with Re when the interface lies at the centreline (Fig. 14a), but the improvement is relatively small, with M increasing from ~ 10% to ~20%. When the interface is offset and is slightly closer to the cylinder (l/W = 0.3), the improvement in mixing is more pronounced, with M reaching approximately 55% at the highest Re examined (Fig. 14b).

The results in this work suggest that a number of competing mechanisms determine the overall mixing efficacy in microchannels with (confined) obstacles; the impact of some of these mechanisms on the mixing performance is sensitive to the position of the fluid interface in relation to the pin. The mechanisms may be summarized as follows:

i) *Diffusion-dominated mixing*: This occurs far upstream of the obstacle and in microchannels without obstacles, and is relatively slow, related to the scalar

(rhodamine) diffusion coefficient in water. It is not significantly affected by the position of the interface (Fig. 14), hence not modified by confinement.

ii) *Steady, three-dimensional convective mixing pre-vortex-shedding:* In flow with obstacles, prior to the onset of vortex-shedding, mixing can be enhanced by transverse flows induced by the pin (Figs. 6c and 6d). They lead to the transport of fluid across the channel, resulting in the appearance of thinner high concentration bands on the lower side of the channel (e.g. Fig. 6g). This is the key mechanism for mixing in low Reynolds number micromixers with obstacles [44]. Optimal mixing in such steady, laminar conditions is attained using arrangements of multiple pins in order to effectively deform the interface and thin/contract one of the two fluid layers creating striations, which in turn enables a stronger diffusive scalar flux across the interface between the two fluids. This multiple pin arrangement however comes to the cost of an increased pressure drop. While being limited to using a single pin, the present study shows that this process is most effective when the interface is offset from the centreline (see Fig. 14 with Re < ~440).

iii) *Unsteady convective mixing, post-vortex-shedding*: When the Reynolds number is sufficiently high, vortex-shedding leads to advective motion and rapid dispersal of the fluid phases throughout the microchannel. In most (but not all) cases, this is the most effective form of mixing (see Fig. 12k). Its efficiency appears to be enhanced when both the interface and the pin are offset from the centreline and are aligned with each other (Fig. 14, δ = 0.42

and l/W = 0.3). This can be intuitively explained by the ability of the pin to efficiently 'break' the diffuse interface (due to molecular diffusion, i.e. mode i) described above) as the latter impinges on the front stagnation point. In a laminar and steady flow without any vortex-shedding, the two fluid layers form shear layers on either side of the pin leading to striations downstream without interacting with each other and resume mixing by diffusion. However, in the case of vortex-shedding, the vortices forming periodically in the wake region of the pin will stretch and distort the two fluid layers before they recombine. This generates thinner concentration structures (striations), promoting higher concentration gradients, and ultimately enhancing the diffusion efficiency and thus mixing.
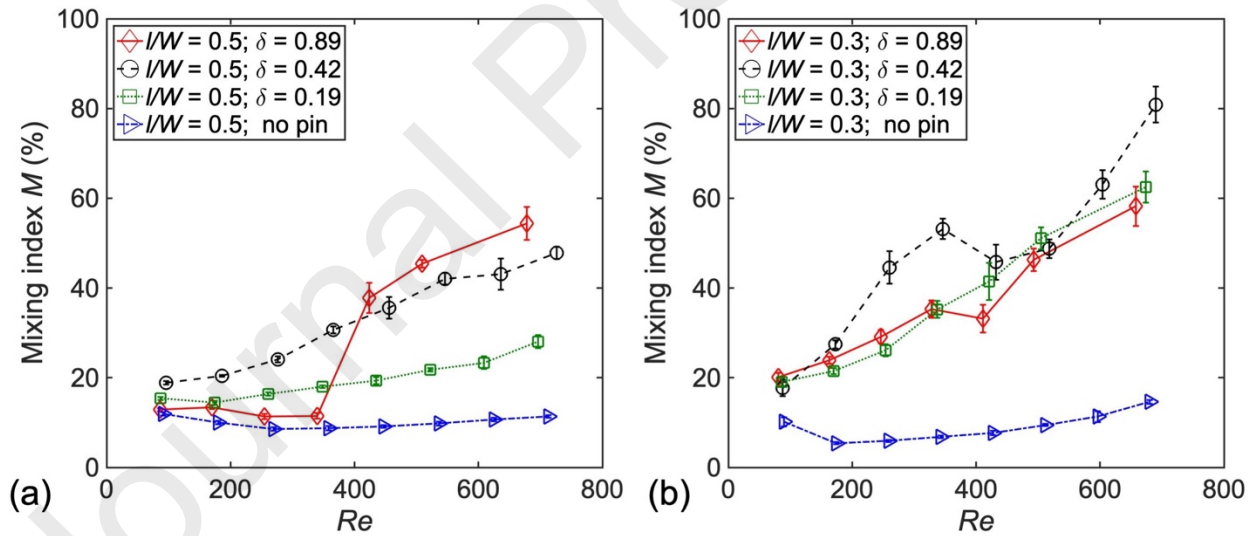

Fig. 14. The relationship between Re and mixing index M downstream of the pin (x/D = 12), l/W = 0.3 and 0.5 as well as various δ. (a) l/W = 0.5 and (b) l/W = 0.3. Note that some of the symbols are larger than the error bars.

4. Conclusion

The mixing of two fluid streams in microchannels with a single, confined cylindrical

obstacle (micropin) has been examined experimentally for various positions of the obstacle and the fluid interface. Two flow ratios are considered at the inlets resulting in the fluid interface positioned on and off the channel centreline (i.e. at half and a third of the channel width respectively). Micro particle image velocimetry is used to characterize the flow around the micropins and micro laser-induced fluorescence system to acquire the instantaneous concentration fields and analyse the mixing performance. When the fluid interface coincides with the channel centreline (I/W = 0.5), i.e. the two fluid streams are mixed at the same ratio, prior to the onset of vortex-shedding, offsetting the pin slightly off the centreline (δ = 0.42) provides the best mixing performance compared to the channels with the pin located on the centreline (δ = 0.89) or nearer the channel wall (δ =0.19). However, when the vortices forming behind the cylindrical pins start shedding, mixing is most efficient when the pin is located on the channel centreline (δ = 0.89), i.e. it is aligned with the interface between the two fluids to be mixed. When the fluid interface is offset from the centreline (I/W = 0.3), optimal mixing is observed when the pin is also offset by the same amount (i.e. for δ = 0.42). Our results indicate that in micromixers involving single obstacles, upon onset of vortex-shedding, shifting the obstacle to lie near the fluid interface improves the mixing performance.

The study elucidates the various mechanisms that determine the mixing in micromixers with a single obstacle. In the absence of obstacle or far upstream of the obstacle, the mixing is diffusion-dominated, and not significantly affected by the position of the fluid interface. At *Re* prior to the onset of vortex-shedding, the presence of obstacles deflects the flow, inducing transverse flow motion and momentum transfer across the channel, leading to the effective dispersal of fluid streams throughout the channel and enhancing mixing. At higher *Re,* exceeding the critical value for the onset

of vortex-shedding from the pin, unsteady convective flows are generated throughout the microchannel as a result of vortex-shedding, providing the most efficient mechanism for mixing at this Re range. Our study suggests two clear strategies for enhanced micromixing when using a confined obstacle (a cylindrical pin): shifting the pin from channel centreline in low Reynolds number range (prior to the onset of vortex-shedding), and aligning the pin axis and the fluid interface at relatively high Reynolds number (following vortex-shedding). We note however that any penalties in the form of rise in pressure drop associated with inclusion of obstacles is not considered here and will require a dedicated investigation in the future. Additionally, the role of multiple pins and parameters such as lateral confinement etc. also need a separate investigation.

Acknowledgments

Appendix A. Supplementary data

Supplementary data to this article can be found in the attachments.

References

[1]   C.-Y. Lee, W.-T. Wang, C.-C. Liu, L.-M. Fu, Passive mixers in microfluidic systems: A review, Chemical Engineering Journal. 288 (2016) 146–160. https://doi.org/10.1016/j.cej.2015.10.122.

[2]   A.-S. Yang, F.-C. Chuang, C.-K. Chen, M.-H. Lee, S.-W. Chen, T.-L. Su, Y.-C. Yang, A high-performance micromixer using three-dimensional Tesla structures for bio-applications, Chemical Engineering Journal. 263 (2015) 444–451. https://doi.org/10.1016/j.cej.2014.11.034.

[3]   H.S. Santana, J.L.S. Júnior, O.P. Taranto, Numerical simulations of biodiesel synthesis in microchannels with circular obstructions, Chemical Engineering and Processing: Process Intensification. 98 (2015) 137–146. https://doi.org/10.1016/j.cep.2015.10.011.

[4]   H. Shi, K. Nie, B. Dong, M. Long, H. Xu, Z. Liu, Recent progress of microfluidic reactors for biomedical applications, Chemical Engineering Journal. 361 (2019) 635–650. https://doi.org/10.1016/j.cej.2018.12.104.

[5]   A. Renfer, M.K. Tiwari, T. Brunschwiler, B. Michel, D. Poulikakos, Experimental investigation into vortex structure and pressure drop across microcavities in 3D integrated electronics, Exp. Fluids. 51 (2011) 731–741. https://doi.org/10.1007/s00348-011-1091-5.

[6]   B. Cantwell, D. Coles, An experimental study of entrainment and transport in the turbulent near wake of a circular cylinder, J. Fluid Mech. 136 (1983) 321. https://doi.org/10.1017/S0022112083002189.

[7]   J.H. Gerrard, The mechanics of the formation region of vortices behind bluff bodies, J. Fluid Mech. 25 (1966) 401–413. https://doi.org/10.1017/S0022112066001721.

[8]   C.H.K. Williamson, Vortex Dynamics in the Cylinder Wake, Annu. Rev. Fluid

Mech. 28 (1996) 477–539. https://doi.org/10.1146/annurev.fl.28.010196.002401.

[9]   A. Renfer, M.K. Tiwari, R. Tiwari, F. Alfieri, T. Brunschwiler, B. Michel, D.

Poulikakos, Microvortex-enhanced heat transfer in 3D-integrated liquid cooling of

electronic chip stacks, Int. J. Heat Mass Transf. 65 (2013) 33–43.

https://doi.org/10.1016/j.ijheatmasstransfer.2013.05.066.

[10]   L. Chen, G. Wang, C. Lim, G.H. Seong, J. Choo, E.K. Lee, S.H. Kang, J.M.

Song, Evaluation of passive mixing behaviors in a pillar obstruction

poly(dimethylsiloxane) microfluidic mixer using fluorescence microscopy, Microfluid

Nanofluid. 7 (2009) 267–273. https://doi.org/10.1007/s10404-008-0386-1.

[11]   S. Zhang, N. Cagney, S. Balabani, C.P. Naveira-Cotta, M.K. Tiwari, Probing

vortex-shedding at high frequencies in flows past confined microfluidic cylinders

using high-speed microscale particle image velocimetry, Physics of Fluids. 31 (2019)

102001. https://doi.org/10.1063/1.5111817.

[12]   N.-T. Nguyen, Z. Wu, Micromixers—a review, J. Micromech. Microeng. 15

(2005) R1–R16. https://doi.org/10.1088/0960-1317/15/2/R01.

[13]   M. Hoffmann, M. Schlüter, N. Räbiger, Experimental investigation of liquid–

liquid mixing in T-shaped micro-mixers using μ-LIF and μ-PIV, Chemical Engineering

Science. 61 (2006) 2968–2976. https://doi.org/10.1016/j.ces.2005.11.029.

[14]   W. Wang, S. Zhao, T. Shao, Y. Jin, Y. Cheng, Visualization of micro-scale

mixing in miscible liquids using μ-LIF technique and drug nano-particle preparation in

T-shaped micro-channels, Chemical Engineering Journal. 192 (2012) 252–261.

https://doi.org/10.1016/j.cej.2012.03.073.

[15]   N. Cagney, S. Balabani, Lagrangian structures and mixing in the wake of a streamwise oscillating cylinder, Phys. Fluids. 28 (2016) 045107. https://doi.org/10.1063/1.4945784.

[16]   N. Aoki, K. Mae, Effects of channel geometry on mixing performance of micromixers using collision of fluid segments, Chemical Engineering Journal. 118 (2006) 189–197. https://doi.org/10.1016/j.cej.2006.02.011.

[17]   F. Alberini, M.J.H. Simmons, A. Ingram, E.H. Stitt, Use of an areal distribution of mixing intensity to describe blending of non-newtonian fluids in a kenics KM static mixer using PLIF, AIChE J. 60 (2014) 332–342. https://doi.org/10.1002/aic.14237.

[18]   C. Powell, Y. Lawryshyn, Modification of Shannon Entropy to Quantify Mixing in UV Reactors, Journal of Environmental Engineering. 143 (2017) 04017068. https://doi.org/10.1061/(ASCE)EE.1943-7870.0001199.

[19]   J. Dusting, S. Balabani, Mixing in a Taylor–Couette reactor in the non-wavy flow regime, Chemical Engineering Science. 64 (2009) 3103–3111. https://doi.org/10.1016/j.ces.2009.03.046.

[20]   A.A.S. Bhagat, E.T.K. Peterson, I. Papautsky, A passive planar micromixer with obstructions for mixing at low Reynolds numbers, Journal of Micromechanics and Microengineering. 17 (2007) 1017–1024. https://doi.org/10.1088/0960-1317/17/5/023.

[21]   L.-Y. Tseng, A.-S. Yang, C.-Y. Lee, C.-Y. Hsieh, CFD-Based Optimization of a Diamond-Obstacles Inserted Micromixer with Boundary Protrusions, Engineering Applications of Computational Fluid Mechanics. 5 (2011) 210–222. https://doi.org/10.1080/19942060.2011.11015365.

[22]   E. Cetkin, A.F. Miguel, Constructal branched micromixers with enhanced mixing efficiency: Slender design, sphere mixing chamber and obstacles,

International Journal of Heat and Mass Transfer. 131 (2019) 633–644.

https://doi.org/10.1016/j.ijheatmasstransfer.2018.11.091.

[23]   T.M. Dundi, V.R.K. Raju, V.P. Chandramohan, Characterization of mixing in

an optimized designed T–T mixer with cylindrical elements, Chinese Journal of

Chemical Engineering. (2019) S1004954118313557.

https://doi.org/10.1016/j.cjche.2019.01.030.

[24]   J.M. Costa, C.P. Naveira-Cotta, Estimation of kinetic coefficients in micro-

reactors for biodiesel synthesis: Bayesian inference with reduced mass transfer

model, Chemical Engineering Research and Design. 141 (2019) 550–565.

https://doi.org/10.1016/j.cherd.2018.11.023.

[25]   P.C. Pontes, C.P. Naveira-Cotta, J.N.N. Quaresma, Three-dimensional

reaction-convection-diffusion analysis with temperature influence for biodiesel

synthesis in micro-reactors, International Journal of Thermal Sciences. 118 (2017)

104–122. https://doi.org/10.1016/j.ijthermalsci.2017.03.022.

[26]   ASTM International, Specification for Biodiesel Fuel Blend Stock (B100) for

Middle Distillate Fuels, ASTM International, 2015. https://doi.org/10.1520/D6751-

15CE01.

[27]   H.S. Santana, J.L. Silva, D.S. Tortola, O.P. Taranto, Transesterification of

sunflower oil in microchannels with circular obstructions, Chinese Journal of

Chemical Engineering. 26 (2018) 852–863.

https://doi.org/10.1016/j.cjche.2017.08.018.

[28]   J.M. Costa Junior, C.P. Naveira-Cotta, D.B. de Moraes, P. Inforçatti Neto, I.A.

Maia, J.V.L. da Silva, H. Alves, M.K. Tiwari, C.G. de Souza, Innovative metallic

microfluidic device for intensified biodiesel production, Ind. Eng. Chem. Res. 59

(2020) 389–398. https://doi.org/10.1021/acs.iecr.9b04892.

[29]   M.A. Ansari, K.-Y. Kim, S.M. Kim, Numerical study of the effect on mixing of the position of fluid stream interfaces in a rectangular microchannel, Microsyst Technol. 16 (2010) 1757–1763. https://doi.org/10.1007/s00542-010-1100-2.

[30]   V. Viktorov, M.R. Mahmud, C. Visconte, Numerical study of fluid mixing at different inlet flow-rate ratios in Tear-drop and Chain micromixers compared to a new H-C passive micromixer, Engineering Applications of Computational Fluid Mechanics. 10 (2016) 182–192. https://doi.org/10.1080/19942060.2016.1140075.

[31]   C. Lei, L. Cheng, S.W. Armfield, K. Kavanagh, Vortex shedding suppression for flow over a circular cylinder near a plane boundary, Ocean Engineering. 27 (2000) 1109–1127. https://doi.org/10.1016/S0029-8018(99)00033-5.

[32]   L. Zovatto, G. Pedrizzetti, Flow about a circular cylinder between parallel walls, J. Fluid Mech. 440 (2001) 1–25. https://doi.org/10.1017/S0022112001004608.

[33]   X.K. Wang, S.K. Tan, Near-wake flow characteristics of a circular cylinder close to a wall, Journal of Fluids and Structures. 24 (2008) 605–627. https://doi.org/10.1016/j.jfluidstructs.2007.11.001.

[34]   A. Bamshad, A. Nikfarjam, H. Khaleghi, A new simple and fast thermally-solvent assisted method to bond PMMA–PMMA in micro-fluidics devices, J. Micromech. Microeng. 26 (2016) 065017. https://doi.org/10.1088/0960-1317/26/6/065017.

[35]   S.-S. Hsieh, J.-W. Lin, J.-H. Chen, Mixing efficiency of Y-type micromixers with different angles, International Journal of Heat and Fluid Flow. 44 (2013) 130–139. https://doi.org/10.1016/j.ijheatfluidflow.2013.05.011.

[36]   A. Soleymani, E. Kolehmainen, I. Turunen, Numerical and experimental investigations of liquid mixing in T-type micromixers, Chemical Engineering Journal. 135 (2008) S219–S228. https://doi.org/10.1016/j.cej.2007.07.048.

[37] M.G. Olsen, R.J. Adrian, Out-of-focus effects on particle image visibility and correlation in microscopic particle image velocimetry, Exp. Fluids. 29 (2000) S166–S174. https://doi.org/10.1007/s003480070018.

[38] J.M. Sherwood, D. Holmes, E. Kaliviotis, S. Balabani, Spatial Distributions of Red Blood Cells Significantly Alter Local Haemodynamics, PLoS ONE. 9 (2014) e100473. https://doi.org/10.1371/journal.pone.0100473.

[39] C. Poelma, A. Kloosterman, B.P. Hierck, J. Westerweel, Accurate Blood Flow Measurements: Are Artificial Tracers Necessary?, PLoS ONE. 7 (2012) e45247. https://doi.org/10.1371/journal.pone.0045247.

[40] H. Bruus, Theoretical microfluidics, Oxford University Press, Oxford; New York, 2008.

[41] S. Pothos, A. Boomsma, D. Troolin, S. Bhattacharya, P. Vlachos, PIV Uncertainty: Computational and Experimental Evaluation of the Peak Ratio Method, in: Volume 2, Fora: Advances in Fluids Engineering Education; Cavitation and Multiphase Flow; Fluid Measurements and Instrumentation, ASME, Washington, DC, USA, 2016: p. V002T10A005. https://doi.org/10.1115/FEDSM2016-7926.

[42] C.T. Culbertson, S.C. Jacobson, J. Michael Ramsey, Diffusion coefficient measurements in microfluidic devices, Talanta. 56 (2002) 365–373. https://doi.org/10.1016/S0039-9140(01)00602-6.

[43] O. Inoue, A. Sakuragi, Vortex shedding from a circular cylinder of finite length at low Reynolds numbers, Phys. Fluids. 20 (2008) 033601. https://doi.org/10.1063/1.2844875.

[44] J. Wang, N. Zhang, J. Chen, V.G.J. Rodgers, P. Brisk, W.H. Grover, Finding the optimal design of a passive microfluidic mixer, Lab Chip. (2019) 10.1039.C9LC00546C. https://doi.org/10.1039/C9LC00546C.

43

Declaration of interests

☒ The authors declare that they have no known competing financial interests or personal relationships that could have appeared to influence the work reported in this paper.

☐The authors declare the following financial interests/personal relationships which may be considered as potential competing interests:

HIGHLIGHTS

- Passive micromixers with confined micropins investigated at high Reynolds numbers.

- Mixing enhancement depends on pin/fluid interface position and vortex-shedding.

- Micro Particle Image Velocimetry and micro Laser Induced Fluorescence employed.

- The convective mixing mechanisms for steady and unsteady flow-regimes elucidated.

44